A Signal-Decomposed and Interference-Annihilated Approach to Hyperspectral Target Detection

Qian Du, *Member, IEEE,* and Chein-I Chang, *Senior Member, IEEE*

***Abstract*—A hyperspectral imaging sensor can reveal and uncover targets with very narrow diagnostic wavelengths. However, it comes at a price that it can also extract many unknown signal sources such as background and natural signatures as well as unwanted man-made objects, which cannot be identified visually or *a priori*. These unknown signal sources can be referred to as interferers, which generally play a more dominant role than noise in hyperspectral image analysis. Separating such interferers from signals and annihilating them subsequently prior to detection may be a more realistic approach. In many applications, the signals of interest can be further divided into desired signals for which we want to extract and undesired signals for which we want to eliminate to enhance signal detectability. This paper presents a signal-decomposed and interference-annihilated (SDIA) approach in applications of hyperspectral target detection. It treats interferers and undesired signals as separate signal sources that can be eliminated prior to target detection. In doing so, a signal-decomposed interference/noise (SDIN) model is suggested in this paper. With the proposed SDIN model, the orthogonal subspace projection-based model and the signal/background/noise model can be included as its special cases. As shown in the experiments, the SDIN model-based SDIA approach generally can improve the performance of the commonly used generalized-likelihood ratio test and constrained energy minimization approach on target detection and classification.**

***Index Terms*—Constrained energy minimization (CEM), generalized-likelihood ratio test (GLRT), interference subspace projection (ISP), orthogonal subspace projection (OSP), signal/background/noise (SBN) model, signal-decomposed and interference-annihilated (SDIA), signal-decomposed and interference/noise (SDIN) model, target-constrained interference-minimized filter (TCIMF).**

I. Introduction

HYPERSPECTRAL imaging has received considerable interest in recent years because it can uncover and reveal subtle spectral characteristics that multispectral sensors cannot resolve. However, it also presents many challenging issues. It has been demonstrated in [1] and [2] that the interference played a more dominant role than did noise in hyperspectral target detection and classification. In many applications, unknown signal sources that are extracted by a hyperspectral imaging sensor cannot be identified visually or *a priori*, e.g., sensor scratches, rocks, roads, water bodies, and other unwanted natural and man-made objects. These types of signal sources are considered as interferers and generally result in severe interfering effects, which further complicates image analysis. Several approaches have been developed to find such interfering sources in an unsupervised manner so that they can be annihilated prior to target detection [3]–[5]. Another type of signal source is signals that are known and have been provided *a priori*. It has been recently shown in [6] that if the signals of interest provided *a priori* are divided into desired and undesired signals, the performance in signal detection/extraction could be enhanced by removal of the undesired signals via orthogonal subspace projection (OSP). This situation often occurs in linear spectral mixture analysis (LSMA) for hyperspectral image analysis [7]–[11], where an image pixel vector is modeled as a linear mixture of a set of signal sources that are assumed to be present in an image scene *a priori*. If those target signal sources can be classified into desired and undesired target signal sources, the hyperspectral target detection can be significantly improved by elimination of the undesired target signal sources prior to the detection of desired target signal sources. This paper presents such a technique, referred to as signal-decomposed and interference-annihilated (SDIA) approach that combines both concepts of interference annihilation in [1] and [2] and signal decomposition proposed in [6].

In order for the SDIA approach to work effectively, we introduce a new sensor signal model, called signal-decomposed and interference/noise (SDIN) model, that classifies signal sources into two signal classes, *a priori* signal sources and *a posteriori* signal sources, where the former is referred to as signals that are known and given *a priori* as opposed to the latter that is signals obtained from the data *a posteriori*. The *a priori* signal sources are further decomposed into desired signals and undesired signals in such a way that the undesired signals can be eliminated to enhance the detection of the desired signals. The *a posteriori* signal sources are usually unknown and can be only extracted by an unsupervised means. They may include a large number of various types of unidentified interfering signal sources. For example, background signatures such as grass and dirts, natural signatures such as trees and rocks, and uninteresting objects such as birds, buildings, and roads, are all considered as *interferers* in this paper. Since all of these interferers as well as *a priori* undesired signal sources present interfering effects on signal detection, they will be referred to as *interference* with respect to *a priori* desired signal sources in this paper. So from a signal detection point of view, the detection

Manuscript received January 28, 2003; revised November 8, 2003. This work was supported in part by the Office of Naval Research under Contract N00014-01-1-0359, in part by the National Research Council under a Senior Research Associateship sponsored by the U.S. Army Soldier and Biological Command, Edgewood Chemical and Biological Center, and in part by an award from the TRW Foundation.

Q. Du is with the Department of Electrical Engineering and Computer Science, Texas A&M University, Kingsville, TX 78363 USA.

C.-I Chang is with the Department of Computer Science and Electrical Engineering, Remote Sensing Signal and Image Processing Laboratory, University of Maryland, Baltimore County, Baltimore, MD 21250 USA.

Digital Object Identifier 10.1109/TGRS.2003.821887

0196-2892/04$20.00 © 2004 IEEE

ability can be increased by annihilation of such interference. The proposed SDIA approach implements the SDIN model to identify these interfering signal sources and annihilate them subsequently from the SDIN model prior to target detection.

Using part of the SDIN model for interference annihilation was explored in [1], where an interference subspace projection (ISP) approach was developed. It made use of an oblique subspace projector to extract the desired signals, while rejecting interference and undesired signals. The idea of treating interference as a separate signal source has been also studied in signal processing [12]–[14]. The proposed SDIA approach can take full advantage of the SDIN model and the interference subspace projection (ISP) in [1] to improve signal detectability.

Interestingly, an alternative approach was recently proposed by Thai and Healey [15], which considered background as a separate signal source. In this case, the standard signal/noise (SN) model was extended to a signal/background/noise (SBN) model that separated target signal sources, background sources, and noise into three individual sources. It then developed a generalized-likelihood ratio test (GLRT) that used a target subspace projector and a background subspace projector as a preprocessing step to suppress effects resulting from noise and background sources before a likelihood ratio test (LRT) is applied to target detection. This approach is different from the proposed SDIA approach in that the SBN-model approach performs signal detection using the GLRT when the noise and background are suppressed, whereas the SDIN model-based SDIA approach performs detection of desired target signals and annihilation of undesired signals and interference without using an LRT. Another difference is that the SBN-model approach generally requires Gaussian noise assumption to produce the LRT, but the SDIN model-based SDIA approach does not. More interestingly, the SDIA approach unifies the interference rejection approach in [1] and the OSP in [6] in the context of *a priori* and *a posteriori* signal sources, while considering the background sources in the SBN model-based GLRT approaches in [15] as a special case of the interference. To be more specific, the target signals considered in the SN and SBN models can be interpreted as *a priori* signals in the SDIN model as opposed to the background sources in the SBN model that can be viewed as interference which is part of *a posteriori* signal sources. Our proposed SDIA approach is based on the SDIN model to combine annihilation of both *a priori* undesired signal sources and *a posteriori* signal sources into one operation and increase signal detectability.

The SDIA approach offers many advantages in versatile applications. When the *a posteriori* signal sources are absent, the SDIA approach is reduced to ISP approach in [1] and the orthogonal subspace projection (OSP) in [6]. On the other hand, if the *a priori* undesired signals are absent and background signals are the only type of *a posteriori* signal sources, the SDIA approach can be considered as a variant of the SBN model-based Thai–Healey approach in [15]. Another advantage benefited from the SDIA approach is its best utilization of the information available from the data. In the standard SN model, the signals of interest are only part of signal sources known *a priori*. There may have *a priori* signal sources that we know but have no interest at all. Such undesired signal sources must be eliminated to avoid their interference in detection performance. In this case, we should be able to take advantage of this prior knowledge to eliminate these *a priori* undesired signals to enhance signal detectability. This practice was exercised previously by the oblique subspace projection in [1], [16]. The SDIA approach makes it more direct and explicit. The OSP approach in [6] was one such method via the SDIA approach to deal with the desired and undesired signal sources separately to improve detection performance. In a similar manner, the target-constrained interference-minimized filter (TCIMF) in [17] also improved the constrained energy minimization (CEM) approach proposed in [18], [19] by eliminating the *a priori* undesired signals instead of minimizing the energies of these signals as the way carried out by the CEM. A third advantage resulting from the SDIA approach is that the GLRT performance can be further improved by including an interference rejection in the GLRT.

The success of SDIA approach mainly depends on how to find and locate *a posteriori* signal sources directly from the data. The automatic target detection and classification algorithm (ATDCA) developed in [4], [5] can be used for this purpose. It can estimate a set of distinct signatures directly from the data in an unsupervised manner. In order to determine how many such *a posteriori* signal sources required to estimate, the method proposed in [20] is further applied to terminate the algorithm. Thai and Healey [15] used singular value decomposition to construct a background subspace that was determined by two parameters. This method will also be investigated in the experiments.

This paper is organized as follows. In Section II, the SDIN model is introduced where methods of estimating the number of *a posteriori* signal sources and finding these signals in the SDIN model are discussed. In Section III, three SDIN model-based SDIA approaches are presented. In Section IV, a series of experiments using computer simulations and real hyperspectral image data are conducted for performance evaluation. In Section V some remarks are concluded.

II. SDIN Model

Given a received signal vector $\mathbf{r}$, a standard signal/noise model is expressed by

$$\mathbf{r} = \mathbf{s} + \mathbf{n} \tag{1}$$

where $\mathbf{s}$ is a known signal vector and $\mathbf{n}$ is the noise vector. Assume that p targets of interest with their associated signatures given by $\mathbf{m}_1, \mathbf{m}_2, \ldots, \mathbf{m}_p$ are present in an image data. We can form a signature matrix $\mathbf{M} = [\mathbf{m}_1, \mathbf{m}_2, \ldots, \mathbf{m}_p]$ with the jth column vector specified by the jth signature $\mathbf{m}_j$. Let $\boldsymbol{\alpha} = (\alpha_1, \alpha_2, \ldots, \alpha_p)^T$ be a $p \times 1$ abundance column vector associated with $\mathbf{r}$, where α_j denotes the abundance fraction of the jth signature $\mathbf{m}_j$ resident in $\mathbf{r}$. If we assume that the spectral signature of an image pixel is a linear mixture of these p signatures, replacing $\mathbf{s}$ in model (1) with $\mathbf{M}\boldsymbol{\alpha}$ yields

$$\mathbf{r} = \mathbf{M}\boldsymbol{\alpha} + \mathbf{n} \tag{2}$$

which is a commonly used linear mixture model in LSMA. Namely, the received signal vector $\mathbf{r}$ in model (1) is now considered as a spectral signature of an image pixel vector in model

(2), which can be modeled as a linear mixture of p target signatures $\mathbf{m}_1, \mathbf{m}_2, \ldots, \mathbf{m}_p$ with their corresponding abundance fractions $\alpha_1, \alpha_2, \ldots, \alpha_p$. Now, if we further assume that we are interested in detecting the pth target with signature $\mathbf{m}_p$, the rest of $p-1$ target signatures will be considered as undesired target signatures. In this case, elimination of these undesired target signatures should improve the detectability of $\mathbf{m}_p$. In order to effectively remove such undesired target signatures, an orthogonal subspace projection (OSP) approach was proposed in [6]. It decomposed the target signature matrix $\mathbf{M}$ in model (2) into the desired target signature $\mathbf{m}_p$ and an undesired target signature matrix $\mathbf{U} = [\mathbf{m}_1, \mathbf{m}_2, \ldots, \mathbf{m}_{p-1}]$, then reformulated model (2) as

$$\mathbf{r} = \mathbf{m}_p \alpha_p + \mathbf{U}\boldsymbol{\gamma} + \mathbf{n} \tag{3}$$

where $\boldsymbol{\gamma} = (\alpha_1, \alpha_2, \ldots, \alpha_{p-1})^T$ is the abundance vector corresponding to $\mathbf{m}_1, \mathbf{m}_2, \ldots, \mathbf{m}_{p-1}$ in $\mathbf{U}$. By virtue of model (3), the OSP has shown its effectiveness in hyperspectral image analysis. In this paper, model (3) will be referred to as OSP-model.

One disadvantage of the OSP model is that it does not take into account background signatures, which generally have significant negative impacts on target detection. Therefore, a recent approach in [15] extended model (2) to the following signal-background-noise (SBN) model for background elimination

$$\mathbf{r} = \mathbf{T}\boldsymbol{\theta} + \mathbf{B}\boldsymbol{\phi} + \mathbf{n} \tag{4}$$

where $\mathbf{T}$ can be considered as the same M in (2) and is a target signal signature matrix consisting of target signal signatures of interest, $\mathbf{B}$ is a background signature matrix, $\boldsymbol{\theta}$ and $\boldsymbol{\phi}$ are the abundance vectors associated with $\mathbf{T}$ and $\mathbf{B}$, respectively. With model (4) a background subspace can be generated and subsequently nulled out by orthogonal projection to improve detection performance. A major difference between the OSP model (3) and SBN model (4) is that the former decomposes target signatures of interest into desired and undesired target signatures and deal with them separately, whereas the latter has mainly focused on background removal.

In what follows, we propose a signal-decomposed and interference/noise (SDIN) model, which combines strengths of both models. It replaces the signal vector $\mathbf{s}$ in model (1) with a three-component signal vector that comprises of *a priori* desired target signatures, *a priori* undesired target signatures and *a posteriori* signatures. More specifically, model (1) can be reexpressed as

$$\mathbf{r} = \mathbf{D}\boldsymbol{\beta} + \mathbf{U}\boldsymbol{\gamma} + \boldsymbol{\Pi}\boldsymbol{\eta} + \mathbf{n} \tag{5}$$

where $\mathbf{D}$ and $\mathbf{U}$ are target signature matrices formed by *a priori* desired and undesired signal signatures, respectively; $\boldsymbol{\beta}$ and $\boldsymbol{\gamma}$ are their corresponding abundance vectors; and $\boldsymbol{\Pi}$ is a matrix made up of *a posteriori* signal signatures with its abundance vector $\boldsymbol{\eta}$. In the SDIN model, the signatures in $\mathbf{D}$ and $\mathbf{U}$ are known and have been provided *a priori*, while the signatures in $\boldsymbol{\Pi}$ need to be generated from the data by an unsupervised method in an *a posteriori* manner and are referred to as *a posteriori* signatures thereafter.

According to the SDIN model specified by model (5), we can interpret various commonly used models as follows. When $\mathbf{M} = [\mathbf{D}\mathbf{U}]$ with $\boldsymbol{\alpha}^T = (\boldsymbol{\beta}^T, \boldsymbol{\gamma}^T)$ and $\boldsymbol{\Pi}$ is absent, model (5) is reduced to the SN model (2). If $\mathbf{D} = \mathbf{m}_p$ with $\boldsymbol{\beta} = \alpha_p$ and $\boldsymbol{\Pi}$ is absent, model (5) is simplified to the OSP model (3). If $\mathbf{D} = \mathbf{T}$ with $\boldsymbol{\beta} = \boldsymbol{\theta}$, $\boldsymbol{\Pi} = \mathbf{B}$ with $\boldsymbol{\eta} = \boldsymbol{\phi}$ and $\mathbf{U}$ is absent, then model (5) becomes the SBN-model (4). In particular, it should bear in mind that the background signature matrix $\mathbf{B}$ in the SBN-model (4) generally is only part of the *a posteriori* signature matrix $\boldsymbol{\Pi}$ considered in model (5). Compared to the signatures in $\mathbf{B}$ used in the SBN model (4) which generally can be identified (e.g., vegetation), the *a posteriori* signatures in $\boldsymbol{\Pi}$ of model (5) may contain more signatures other than background signatures, such as natural signatures (e.g., trees, rocks), uninteresting objects (e.g., sensor scratches, birds, buildings, roads), and signatures that cannot even be identified. In this paper, we adopt the term of "interferer" to represent any unknown signature that is not of interest and causes interfering effects on target detection. In the light of this interpretation, the *a priori* undesired and *a posteriori* signatures together are considered as "interference." Therefore, the $\mathbf{B}$ can be viewed as part of signal sources in $\boldsymbol{\Pi}$. For simplicity and clarity, we denote the *a priori* desired signatures and the *a priori* undesired target signatures by $\mathbf{d}_1, \mathbf{d}_2, \ldots, \mathbf{d}_{n_\mathbf{D}}$ in $\mathbf{D}$ and $\mathbf{u}_1, \mathbf{u}_2, \ldots, \mathbf{u}_{n_\mathbf{U}}$ in $\mathbf{U}$ respectively, and the *a posteriori* signatures by $\boldsymbol{\pi}_1, \boldsymbol{\pi}_2, \ldots, \boldsymbol{\pi}_{n_\Pi}$ in $\boldsymbol{\Pi}$.

In order to effectively work on model (5), we need to determine the number of *a posteriori* signatures in $\boldsymbol{\Pi}$, i.e., n_Π, and the interference signatures $\boldsymbol{\pi}_1, \boldsymbol{\pi}_2, \ldots, \boldsymbol{\pi}_{n_\Pi}$ in $\boldsymbol{\Pi}$, which are generally unknown *a priori*. In the following section, we suggest a Neyman–Pearson detection theory-based eigenthresholding method proposed in [20] to estimate the number of distinct signals and an unsupervised target generation algorithm developed in [4] to find these *a posteriori* signatures to form $\boldsymbol{\Pi}$.

A. Estimation of Number of A Posteriori Signatures

Let $\mathbf{K}$ be the data sample covariance matrix and $\mathbf{K}_n$ the noise variance matrix. The $\mathbf{K}_n$ can be estimated using the linear prediction method in [21]. First, each band image is divided into nonoverlapping blocks. Second, each pixel is linearly predicted using its spatial and spectral neighbors, and in each block the optimal linear prediction scheme is applied. Third, the prediction error in each block can be considered as the noise variance in that block, while the noise variance in a band image can be estimated by averaging the noise variances in all the blocks. It should be noted that the resulting $\mathbf{K}_n$ is a diagonal matrix with the kth element corresponding to the noise variance in the kth band image. The noise-whitened $\overline{\mathbf{K}}$ can be obtained by $\mathbf{K}_n^{-1/2}\mathbf{K}\mathbf{K}_n^{-1/2}$. As a result, the noise variance of each band in $\overline{\mathbf{K}}$ is reduced to unity.

Let $\{\mathbf{a}_k\}_{k=1}^{L}$ be a set of eigenvalues generated by the eigendecomposition of $\overline{\mathbf{K}}$. We can express $\overline{\mathbf{K}}$ as

$$\overline{\mathbf{K}} = \sum_{k=1}^{n_\mathbf{D}+n_\mathbf{U}+n_\mathbf{\Pi}} \lambda_k \mathbf{a}_k \mathbf{a}_k^T + \sum_{k=n_\mathbf{D}+n_\mathbf{U}+n_\mathbf{\Pi}+1}^{L} \lambda_k \mathbf{a}_k \mathbf{a}_k^T \tag{6}$$

where $\{\mathbf{a}_k\}_{k=1}^{n_\mathbf{D}+n_\mathbf{U}+n_\mathbf{\Pi}}$ and $\{\mathbf{a}_k\}_{k=n_\mathbf{D}+n_\mathbf{U}+n_\mathbf{\Pi}+1}^{L}$ span the *a priori*/*a posteriori* signal subspace and noise subspace, respectively. Since the noise covariance matrix in the noise-whiten data is an identity matrix, the noise contribution to all the eigenvalues of $\overline{\mathbf{K}}$ are unity. The eigenvalue λ_k, for $k = n_\mathbf{D} + n_\mathbf{U} +$

$n_\Pi + 1, \ldots, L$, containing noise only is one, while eigenvalue λ_k, for $k = 1, \ldots, n_{\mathbf{D}} + n_{\mathbf{U}} + n_\Pi$, containing signal and noise is larger than one. More precisely, the eigenvalues of $\overline{\mathbf{K}}$ can be represented by

$$\begin{aligned} \lambda_k &> 1, \qquad k = 1, \ldots, n_{\mathbf{D}} + n_{\mathbf{U}} + n_{\mathbf{\Pi}} \\ \lambda_k &= 1, \qquad k = n_{\mathbf{D}} + n_{\mathbf{U}} + n_{\mathbf{\Pi}} + 1, \ldots, L. \end{aligned} \tag{7}$$

Now, using the results in [22], we can model the kth eigenvalue λ_k as a random variable z_k for $k = 1, 2, \ldots, L$, which abides by the Gaussian distribution. Then, the estimation of $n_{\mathbf{D}} + n_{\mathbf{U}} + n_\Pi$ can be formulated as a following binary hypothesis-testing problem

$$H_0 : z_k = 1 \text{ versus } H_1 : z_k > 1, \qquad k = 1, 2, \ldots, L \tag{8}$$

where the null hypothesis H_0 and the alternative hypothesis H_1 represent the cases of signal absence and signal presence, respectively. The probability density functions under hypotheses H_0 and H_1 are given by

$$p_0(z_k) = p(z_k|H_0) \cong \mathcal{N}\left(1, \sigma_{z_k}^2\right), \qquad k = 1, 2, \ldots, L \tag{9}$$

$$p_1(z_k) = p(z_k|H_1) \cong \mathcal{N}\left(\mu_{z_k}, \sigma_{z_k}^2\right), \qquad k = 1, 2, \ldots, L \tag{10}$$

respectively, where μ_{z_k} and $\sigma_{z_k}^2$ are the mean and variance of the random variable z_k.

It has been shown in [22] that when the total number of pixel vectors, N, is sufficiently large, the noise variance $\sigma_{z_k}^2$ in (9) and (10) can be estimated by

$$\sigma_{z_k}^2 = \text{Var}[z_k] \approx \frac{2\lambda_k^2}{N}, \qquad k = 1, 2, \ldots, L. \tag{11}$$

By means of (9)–(11) we arrive at a Neyman–Pearson detector δ_{NP} for the binary composite hypothesis testing problem in (8) as below [23]

$$\delta_{\text{NP}} = \begin{cases} 1, & L(z_k) > \tau_k \\ 1 \text{ with probability } q, & L(z_k) = \tau_k \\ 0, & L(z_k) < \tau_k \end{cases}, \qquad k = 1, 2, \ldots, L \tag{12}$$

where $L(z_k) = (p_1(z_k)/p_0(z_k))$ is the likelihood ratio test, q is the probability of saying H_1 when $L(z_k) = (p_1(z_k)/p_0(z_k)) = \tau_k$, and the threshold τ_k is determined by the false-alarm probability α given by

$$\int\limits_{\{L(z_k) > \tau_k\}} p_0(z_k) dz_k = \alpha, \qquad k = 1, 2, \ldots, L. \tag{13}$$

The detector specified by (12) can be used to determine the $n_{\mathbf{D}} + n_{\mathbf{U}} + n_\Pi$ by counting how many times δ_{NP} fails the test. Each failure is caused by the presence of a signal source in the data. In particular, when the detector δ_{NP} passes the kth test, that is, $\mu_k = 1$, it implies that the noise is the only source contributed to the energy in the kth eigenvalue. In other words, there is no signal energy present in the kth eigenvalue. As soon as $n_{\mathbf{D}} + n_{\mathbf{U}} + n_\Pi$ is estimated, the n_Π can be obtained by subtracting $n_{\mathbf{D}} + n_{\mathbf{U}}$ from the estimated $n_{\mathbf{D}} + n_{\mathbf{U}} + n_\Pi$. It should be noted that such hypothesis testing is performed for each eigenvalue represented by z_k. Since this is a constant false-alarm rate (CFAR) detection problem and $p_0(z_k)$ is the same for each k, τ_k is the same for each k. So here the subscript k can be suppressed.

B. Algorithm for Finding A Posteriori Signatures

After the n_Π is determined, we need to locate and find these *a posteriori* signatures. The following approach suggested in [4] and further studied in [5] can be used for this purpose.

Since the $n_{\mathbf{D}}$ desired target signatures $\mathbf{d}_1, \mathbf{d}_2, \ldots, \mathbf{d}_{n_{\mathbf{D}}}$ and the $n_{\mathbf{U}}$ undesired target signatures $\mathbf{u}_1, \mathbf{u}_2, \ldots, \mathbf{u}_{n_{\mathbf{U}}}$ are available *a priori*, we use them as the initial set of targets. We then define an orthogonal subspace projector $P_{[\mathbf{DU}]}^\perp = \mathbf{I}_{\text{identity}} - [\mathbf{DU}][\mathbf{DU}]^\#$, where $\mathbf{I}_{\text{identity}}$ is the $L \times L$ identity matrix and $[\mathbf{DU}]^\# = ([\mathbf{DU}]^T[\mathbf{DU}])^{-1}[\mathbf{DU}]^T$ is the pseudo-inverse of $[\mathbf{DU}]$ and the superscript "T" denotes matrix transpose operation. The $P_{[\mathbf{DU}]}^\perp$ will be used to project all image pixel vectors into the orthogonal complement subspace, denoted by $\langle \mathbf{D}, \mathbf{U} \rangle^\perp$, which is orthogonal to the subspace $\langle \mathbf{D}, \mathbf{U} \rangle$ that is linearly spanned by $\mathbf{D}$ and $\mathbf{U}$. The maximum length of a pixel vector in $\langle \mathbf{D}, \mathbf{U} \rangle^\perp$ that corresponds to the maximum orthogonal projection with respect to $\langle \mathbf{D}, \mathbf{U} \rangle$ will be selected as a first *a posteriori* signature denoted by $\boldsymbol{\pi}_1$. The reason for this selection is that the selected $\boldsymbol{\pi}_1$ will have the most distinct features from the target signatures represented by $\langle \mathbf{D}, \mathbf{U} \rangle$ in the sense of orthogonal projection, because $\boldsymbol{\pi}_1$ has the largest magnitude of the projection in $\langle \mathbf{D}, \mathbf{U} \rangle^\perp$ produced by $P_{[\mathbf{DU}]}^\perp$. A new orthogonal subspace projector $P_{[\mathbf{DU}\boldsymbol{\pi}_1]}^\perp$ is then constructed and applied to the image to generate a second a posteriori signature $\boldsymbol{\pi}_2$. Once again, the pixel vector with maximum length in $\langle \mathbf{D}, \mathbf{U}, \boldsymbol{\pi}_1 \rangle^\perp$ that is orthogonal to $[\mathbf{DU}]$ and $\boldsymbol{\pi}_1$ will be selected as $\boldsymbol{\pi}_2$. The above procedure will be repeated to find a third target $\boldsymbol{\pi}_3$, a fourth target $\boldsymbol{\pi}_4$, etc., until the n_Πth *a posteriori* signature π_{n_Π} is found when the algorithm can be terminated.

III. SDIA Approaches to Target Detection

In this section, we introduce three SDIN model-based SDIA approaches to target detection, which are derived from the GLRT, the CEM in [17], and ISP in [1]. In addition, the method developed by Thai and Healey in [15] will be also described in this section for comparative analysis.

A. GLRT-Based SDIA Approach

The likelihood ratio test is a standard detection method and has been widely used in signal processing community. With the traditional SN model replaced by the SDIN model, an SDIN-model based detection problem can be cast as follows:

$$H_0 : \mathbf{r} = \mathbf{U}\boldsymbol{\alpha}_{\mathbf{U}} + \mathbf{\Pi}\boldsymbol{\alpha}_{\mathbf{\Pi}} + \mathbf{n} = \mathbf{\Psi}\boldsymbol{\alpha}_{\mathbf{\Psi}} + \mathbf{n}$$

versus

$$H_1 : \mathbf{r} = \mathbf{D}\boldsymbol{\alpha}_{\mathbf{D}} + \mathbf{U}\boldsymbol{\alpha}_{\mathbf{U}} + \mathbf{\Pi}\boldsymbol{\alpha}_{\mathbf{\Pi}} + \mathbf{n} = \mathbf{S}\boldsymbol{\alpha}_{\mathbf{S}} + \mathbf{n} \tag{14}$$

where $\mathbf{\Psi} = [\mathbf{U}\ \mathbf{\Pi}]$ is referred to as the interference signature matrix made up of the *a priori* undesired signatures and *a posteriori* signatures with its abundance vector denoted by $\boldsymbol{\alpha}_{\mathbf{\Psi}}^T = (\boldsymbol{\alpha}_{\mathbf{U}}^T \boldsymbol{\alpha}_{\mathbf{\Pi}}^T)$; $\mathbf{S} = [\mathbf{D}\ \mathbf{U}\ \mathbf{\Pi}]$ is the entire signature matrix consisting of all *a priori* and *a posteriori* signal signatures, and $\boldsymbol{\alpha}_{\mathbf{S}}^T = (\boldsymbol{\alpha}_{\mathbf{D}}^T \boldsymbol{\alpha}_{\mathbf{U}}^T \boldsymbol{\alpha}_{\mathbf{\Pi}}^T)$ is its corresponding abundance vector. When

$\mathbf{n}$ is additive zero-mean Gaussian noise, the maximum-likelihood estimates of $\boldsymbol{\alpha}_{\boldsymbol{\Psi}}$ and $\boldsymbol{\alpha}_{\mathbf{S}}$ can be obtained by

$$\boldsymbol{\alpha}_{\boldsymbol{\Psi}} = (\boldsymbol{\Psi}^T\boldsymbol{\Psi})^{-1}\boldsymbol{\Psi}^T\mathbf{r} \tag{15}$$

$$\boldsymbol{\alpha}_{\mathbf{S}} = (\mathbf{S}^T\mathbf{S})^{-1}\mathbf{S}^T\mathbf{r}. \tag{16}$$

If the noise in (14) is further assumed to be white with its covariance matrix denoted by $\sigma^2\mathbf{I}_{\text{identity}}$, the maximum-likelihood estimates of σ^2 under the two hypotheses in (14) can be derived as [12]

$$\hat{\sigma}_0^2 = \frac{\|\mathbf{r}-\boldsymbol{\Psi}\hat{\boldsymbol{\alpha}}_{\boldsymbol{\Psi}}\|^2}{L} = \frac{\|\mathbf{r}-P_{\boldsymbol{\Psi}}\mathbf{r}\|^2}{L} = \frac{\|P_{\boldsymbol{\Psi}}^{\perp}\mathbf{r}\|^2}{L} = \frac{\mathbf{r}^T P_{\boldsymbol{\Psi}}^{\perp}\mathbf{r}}{L} \tag{17}$$

$$\hat{\sigma}_1^2 = \frac{\|\mathbf{r}-\mathbf{S}\hat{\boldsymbol{\alpha}}_{\mathbf{S}}\|^2}{L} = \frac{\|\mathbf{r}-P_{\mathbf{S}}\mathbf{r}\|^2}{L} = \frac{\|P_{\mathbf{S}}^{\perp}\mathbf{r}\|^2}{L} = \frac{\mathbf{r}^T P_{\mathbf{S}}^{\perp}\mathbf{r}}{L} \tag{18}$$

where $P_{\boldsymbol{\Psi}} = \boldsymbol{\Psi}(\boldsymbol{\Psi}^T\boldsymbol{\Psi})^{-1}\boldsymbol{\Psi}^T$ and $P_{\mathbf{S}} = \mathbf{S}(\mathbf{S}^T\mathbf{S})^{-1}\mathbf{S}^T$ are the interference signature subspace projector and entire signature subspace projector, respectively, while $P_{\boldsymbol{\Psi}}^{\perp} = \mathbf{I}_{\text{identity}} - \boldsymbol{\Psi}(\boldsymbol{\Psi}^T\boldsymbol{\Psi})^{-1}\boldsymbol{\Psi}^T$ and $P_{\mathbf{S}}^{\perp} = \mathbf{I}_{\text{identity}} - \mathbf{S}(\mathbf{S}^T\mathbf{S})^{-1}\mathbf{S}^T$ are annihilators of the subspaces $\boldsymbol{\Psi}$ and $\mathbf{S}$, respectively. Using (15)–(18) their associated probability density functions can be found by

$$p_0(\mathbf{r}) = p(\mathbf{r}|H_0) \cong \mathcal{N}\left(\boldsymbol{\Pi}\hat{\boldsymbol{\alpha}}_{\boldsymbol{\Psi}}, \hat{\sigma}_0^2\mathbf{I}_{\text{identity}}\right) = \mathcal{N}\left(P_{\boldsymbol{\Psi}}\mathbf{r}, \hat{\sigma}_0^2\mathbf{I}_{\text{identity}}\right) \tag{19}$$

$$p_1(\mathbf{r}) = p(\mathbf{r}|H_1) \cong \mathcal{N}\left(\mathbf{S}\hat{\boldsymbol{\alpha}}_{\mathbf{S}}, \hat{\sigma}_1^2\mathbf{I}_{\text{identity}}\right) = \mathcal{N}\left(P_{\mathbf{S}}\mathbf{r}, \hat{\sigma}_1^2\mathbf{I}_{\text{identity}}\right). \tag{20}$$

Finally, the generalized log-likelihood ratio $\Lambda(\mathbf{r})$ resulting from (19) and (20) can be obtained by

$$(\Lambda(\mathbf{r}))^{2/L} = \frac{\mathbf{r}^T P_{\boldsymbol{\Psi}}^{\perp}\mathbf{r}}{\mathbf{r}^T P_{\mathbf{S}}^{\perp}\mathbf{r}}. \tag{21}$$

A detector using (21) can be applied to detect the target signatures $\mathbf{d}_1, \mathbf{d}_2, \ldots, \mathbf{d}_{n_{\mathbf{D}}}$ in $\mathbf{D}$ that are present in the pixel $\mathbf{r}$. For a special case of single-target detection, the desired target signature matrix $\mathbf{D}$ in (14) can be replaced by the desired target signature $\mathbf{d}$ to achieve the detection of $\mathbf{d}$.

B. Thai–Healey Method

In recent report [15], a target/background/noise model, here referred to as SBN model, was proposed. It extended the standard SN model by considering target signals, background signatures, and noise as three separate information sources. Since the background sources are *a posteriori* signal sources and can be regarded as part of interferers in the context of the SDIN model, the SDIN model includes the SBN model as its special case, where the undesired target signature matrix $\mathbf{U}$ is absent in the model (5). Instead of the algorithm described in Section II-B that we applied to find *a posteriori* signatures, the method in [15] intended to construct the background subspace $\langle\mathbf{B}\rangle$. An appropriate background data matrix $\mathbf{Y}$ that did not include the target pixels was required for this purpose. More precisely, each image pixel vector $\mathbf{r}$ was examined using the similarity criterion defined as

$$\gamma_i(\mathbf{r}) = \frac{\|\mathbf{d}_i^T\mathbf{r}\|}{\mathbf{r}^T\mathbf{r}}, \qquad \mathbf{d}_i,\ 1 \le i \le p \tag{22}$$

where $\mathbf{d}_1, \mathbf{d}_2, \ldots, \mathbf{d}_{n_{\mathbf{D}}}$ are desired target signatures that formed the target subspace. If $\gamma_i(\mathbf{r}) > \gamma_0$ with γ_0 set to a prescribed similarity threshold, the pixel vector $\mathbf{r}$ would be considered as a candidate target pixel and be removed from $\mathbf{Y}$. After the background data matrix $\mathbf{Y}$ was formed, the singular value decomposition (SVD) was then applied to find significant eigenvalues, and their corresponding eigenvectors that would be used as basis vectors of $\langle\mathbf{B}\rangle$. The number of basis vectors $n_{\langle\mathbf{B}\rangle}$ used in the construction of $\langle\mathbf{B}\rangle$, was determined by two thresholds that were selected based on a variance-based band power ratio using a technique similar to that proposed in [24]. Then, the first $n_{\langle\mathbf{B}\rangle}$ eigenvectors $\mathbf{b}_1^e, \mathbf{b}_2^e, \ldots, \mathbf{b}_{n_{\langle\mathbf{B}\rangle}}^e$ formed a background eigenvector matrix $\mathbf{B}^e = [\mathbf{b}_1^e, \mathbf{b}_2^e, \ldots, \mathbf{b}_{n_{\langle\mathbf{B}\rangle}}^e]$. Let the background subspace projector be defined by $P_{\mathbf{B}}^{\perp} = \mathbf{I}_{\text{identity}} - (\mathbf{B}^e)(\mathbf{B}^e)^T$. Substituting $P_{\mathbf{B}}^{\perp}$ for $P_{\boldsymbol{\Psi}}^{\perp}$ in (21) results in

$$(\Lambda(\mathbf{r}))^{\frac{2}{L}} = \frac{\mathbf{r}^T P_{\mathbf{B}}^{\perp}\mathbf{r}}{\mathbf{r}^T P_{\mathbf{S}}^{\perp}\mathbf{r}} \tag{23}$$

which is exactly the GLRT detector derived by the method in [15].

Several comments are noteworthy.

1) The Thai–Healey method can be considered as a variant of the GLRT method in Section III-A, where the noise is assumed to be Gaussian. If the noise is non-Gaussian, no closed-form solution can be derived.
2) The background eigenvector matrix $\mathbf{B}^e$ is not made up of individual background signatures. Instead, it consists of eigenvectors that span the background subspace $\langle\mathbf{B}\rangle$. As a result, there is no need to find all background signatures. The key issue is to determine an appropriate number of background eigenvectors $n_{\langle\mathbf{B}\rangle}$ that spans the $\langle\mathbf{B}\rangle$. If it is too small, $\langle\mathbf{B}\rangle$ will be under represented. But if $n_{\langle\mathbf{B}\rangle}$ is too large, target signatures that are not orthogonal to background signatures will be forced to be considered as background signatures. In this case, some target components will be eliminated prior to detection. As a result, the Thai–Healey method may perform poorly.
3) In order to make sure that target pixels are excluded from the construction of $\langle\mathbf{B}\rangle$, all the target candidate pixels must be checked by (22) with an empirically selected threshold γ_0. In this case, γ_0 must be carefully determined. The determination of γ_0 is difficult when no pure target pixels are present in an image scene.
4) The Thai–Healey method can be easily extended by the proposed SDIA approach via the SDIN model with undesired targets and background signatures interpreted as *a priori* and *a posteriori* signal sources, respectively. In the experiments, we will demonstrate that an SDIN model-based Thai–Healey method can outperform its counterpart using the SBN model provided that $n_{\langle\mathbf{B}\rangle}$ and γ_0 are appropriately selected. When there are no *a priori*

undesired signals, the SDIN model-based Thai–Healey method is reduced to the original Thai–Healey method.

C. CEM-Based SDIA Approach

The CEM approach has shown success in hyperspectral target detection [18], [19]. It is a matched filter-based technique, which is designed to extract a specific desired target. For a particular target $\mathbf{d}_i$, a CEM-based filter is a linear filter specified by a set of filter coefficients given by $\mathbf{w}_i = (w_{i1}, w_{i2}, \ldots, w_{iL})^T$ that minimizes its output energy

$$E = \sum_k \left(\mathbf{w}_i^T \mathbf{r}_k\right)^T \left(\mathbf{w}_i^T \mathbf{r}_k\right) = \sum_k \left(\mathbf{w}_i^T \mathbf{r}_k\right)^2 \tag{24}$$

where $\{\mathbf{r}_k\}$ is the set of image pixel vectors. The $\mathbf{w}$ is to be found for extracting the target $\mathbf{d}_i$ by imposing the following linear constraint

$$\mathbf{w}_i^T \mathbf{d}_i = 1. \tag{25}$$

In other words, a CEM filter design is to find an optimal filter coefficient vector $\mathbf{w}_i^{\mathrm{CEM}}$ that solves the following constrained problem:

$$\min_{\mathbf{w_i}} E \text{ subject to } \mathbf{w}_i^T \mathbf{d}_i = 1. \tag{26}$$

The solution to (26) is given by

$$\mathbf{w}_i^{\mathrm{CEM}} = \frac{\mathbf{d}_i^T \mathbf{R}^{-1}}{\mathbf{d}_i^T \mathbf{R}^{-1} \mathbf{d}_i} \tag{27}$$

where $\mathbf{R}$ is the sample spectral correlation matrix given by $(1/N)\sum_k \mathbf{r}_k \mathbf{r}_k^T$ and N is the number of image pixel vectors in $\{\mathbf{r}_k\}$. The CEM detector, $\delta^{\mathrm{CEM}}(\mathbf{r})$ derived in [18], is specified by the weight vector $\mathbf{w}^{\mathrm{CEM}}$ in (27) and given by

$$\delta^{\mathrm{CEM}}(\mathbf{r}) = \left(\mathbf{w}^{\mathrm{CEM}}\right)^T \mathbf{r}. \tag{28}$$

The CEM filter specified by (28) is based on the SN model. It can be extended to the SDIN model by introducing a second constraint that can be used to eliminate the effects caused by the interference signatures in $\mathbf{\Psi}$ by imposing

$$\mathbf{w}_i^T \mathbf{\Psi} = \mathbf{0}_{(n_{\mathbf{U}}+n_{\mathbf{\Pi}})\times 1}^T \tag{29}$$

where $\mathbf{0}_{(n_{\mathbf{U}}+n_{\mathbf{\Pi}})\times 1}$ is the $(n_{\mathbf{U}} + n_{\mathbf{\Pi}}) \times 1$ zero vector with all the elements equal to 0. Combining the constraint (25) and (29) yields the following joint constraint equation

$$\mathbf{w}_i^T [\mathbf{d}_i \ \mathbf{\Psi}] = \left[1 \ \mathbf{0}_{(n_{\mathbf{U}}+n_{\mathbf{\Pi}})\times 1}^T\right]. \tag{30}$$

Substituting (30) for (25) in (26) results in an extended version of (26)

$$\min_{\mathbf{w}_i} E \text{ subject to } \mathbf{w}_i^T [\mathbf{d}_i \ \mathbf{\Psi}] = \left[1 \ \mathbf{0}_{(n_{\mathbf{U}}+n_{\mathbf{\Pi}})\times 1}^T\right]. \tag{31}$$

The solution to (31) can be used to extract target $\mathbf{d}_i$, while eliminating the interference signatures in $\mathbf{\Psi}$. Additionally, (31) can be further extended to detect multiple target signatures $\mathbf{d}_1, \mathbf{d}_2, \ldots, \mathbf{d}_{n_{\mathbf{D}}}$ in $\mathbf{D}$ by implementing the following constraint equation

$$\mathbf{w}^T \mathbf{S} = \begin{bmatrix} \mathbf{1}_{n_{\mathbf{D}}\times 1} \\ \mathbf{0}_{(n_{\mathbf{U}}+n_{\mathbf{\Pi}})\times 1} \end{bmatrix}^T \tag{32}$$

where $\mathbf{1}_{n_{\mathbf{D}}\times 1}$ is the $n_{\mathbf{D}} \times 1$ unity vector with all the elements equal to 1. The solution to this new constrained problem $\mathbf{w}^{\mathrm{TCIMF}}$ is given by

$$\mathbf{w}^{\mathrm{TCIMF}} = \mathbf{R}^{-1}\mathbf{S}(\mathbf{S}^T\mathbf{R}^{-1}\mathbf{S})^{-1} \begin{bmatrix} \mathbf{1}_{n_{\mathbf{D}}\times 1} \\ \mathbf{0}_{(n_{\mathbf{U}}+n_{\mathbf{\Pi}})\times 1} \end{bmatrix}. \tag{33}$$

Using $\mathbf{w}^{\mathrm{TCIMF}}$ in (33), we can obtain the following filter, referred to as the target-constrained interference-minimized filter, developed in [17]:

$$\delta^{\mathrm{TCIMF}}(\mathbf{r}) = \left(\mathbf{w}^{\mathrm{TCIMF}}\right)^T \mathbf{r}. \tag{34}$$

D. ISP-Based SDIA Approach

The likelihood ratio test given by (21) requires the prior knowledge of probability distributions under each hypothesis, which are obtained by assuming that the noise is an additive Gaussian process. However, it is generally not true for most remotely sensed images. The ISP method presented in this section does not need such knowledge or make any assumption about the distribution. It finds a projector specified by $\mathbf{w}_i^{\mathrm{ISP}}$ that maximizes the SNR over $\mathbf{w}_i$ in the subspace $\langle\mathbf{\Psi}\rangle^{\perp}$ that is orthogonal to the interference signature subspace $\langle\mathbf{\Psi}\rangle$. First of all, the pixel vector $\mathbf{r}$ is projected via $P_{\mathbf{\Psi}}^{\perp}$ onto the orthogonal interference signature subspace $\langle\mathbf{\Psi}\rangle^{\perp}$ to annihilate the interference signatures. As a result, (3) becomes

$$P_{\mathbf{\Psi}}^{\perp}\mathbf{r} = P_{\mathbf{\Psi}}^{\perp}\mathbf{d}_i\alpha_{\mathbf{d_i}} + P_{\mathbf{\Psi}}^{\perp}\mathbf{n}. \tag{35}$$

Then, we search for an optimal vector $\mathbf{x}_i^*$ that maximizes the SNR in the $\langle\mathbf{\Psi}\rangle^{\perp}$ given by

$$\mathrm{SNR}_i = \frac{\alpha_{\mathbf{d_i}}^2}{\sigma^2} \frac{\mathbf{x}_i^T P_{\mathbf{\Psi}}^{\perp}\mathbf{d}_i\mathbf{d}_i^T P_{\mathbf{\Psi}}^{\perp}\mathbf{x}_i}{\mathbf{x}_i^T P_{\mathbf{\Psi}}^{\perp}\mathbf{x}_i}. \tag{36}$$

Finding the optimal $\mathbf{x}_i^*$ is equivalent to solving the following eigenvalue problem:

$$\mathbf{d}_i\mathbf{d}_i^T P_{\mathbf{\Psi}}^{\perp}\mathbf{x}_i = \lambda_i\mathbf{x}_i. \tag{37}$$

The maximum eigenvalue $\lambda_i^{\max}$ of $\mathbf{d}_i\mathbf{d}_i^T P_{\mathbf{\Psi}}^{\perp}$ is the one achieving the maximum SNR and its corresponding eigenvector is the desired optimal projection vector $\mathbf{x}_i^*$. Because the rank of $\mathbf{d}_i\mathbf{d}_i^T P_{\mathbf{\Psi}}^{\perp}$ is one, $\lambda_i^{\max}$ is the only nonzero eigenvalue. Furthermore, since $\lambda_i^{\max} = \mathrm{trace}\{\mathbf{d}_i\mathbf{d}_i^T P_{\mathbf{\Psi}}^{\perp}\} = \mathrm{trace}\{\mathbf{d}_i^T P_{\mathbf{\Psi}}^{\perp}\mathbf{d}_i\} = \mathbf{d}_i^T P_{\mathbf{\Psi}}^{\perp}\mathbf{d}_i$, (37) becomes

$$\mathbf{d}_i\mathbf{d}_i^T P_{\mathbf{\Psi}}^{\perp}\mathbf{x}_i = \mathbf{d}_i^T P_{\mathbf{\Psi}}^{\perp}\mathbf{d}_i\mathbf{x}_i \tag{38}$$

with the solution given by

$$\mathbf{x}_i^* = \beta_i\mathbf{d}_i \tag{39}$$

where β_i is a constant. The form in (39) is identical to that of the OSP classifier derived in [6] except that the undesired target

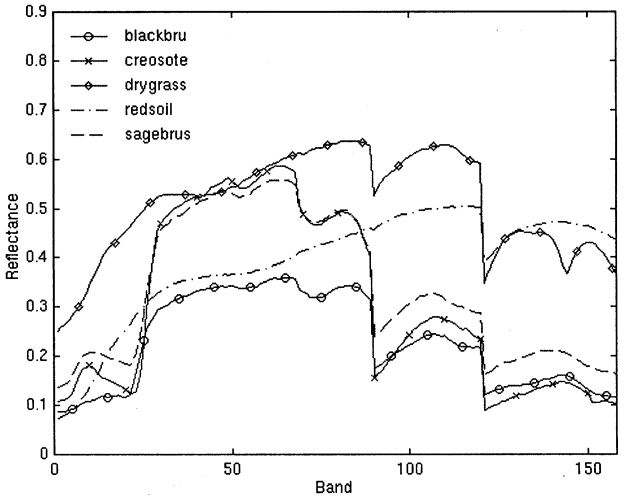

Fig. 1. Spectra of AVIRIS five signatures.

signature matrix $\mathbf{U}$ in the OSP classifier is replaced by interference signature matrix $\mathbf{\Psi}$. In order to account for the abundance estimation error, the constant β_i can be determined in a similar manner that was done in the *a posteriori* OSP in [16] and is given by

$$\beta_i = \frac{1}{\mathbf{d}_i^T P_{\mathbf{\Psi}}^{\perp} \mathbf{d}_i}. \tag{40}$$

Using $P_{\mathbf{\Psi}}^{\perp}$ and (39) and (40), the ISP detector $\delta^{\mathrm{ISP}}(\mathbf{r})$ can be derived by

$$\delta^{\mathrm{ISP}}(\mathbf{r}) = \left(\mathbf{d}_i^T P_{\mathbf{\Psi}}^{\perp} \mathbf{d}_i\right)^{-1} \mathbf{d}_i^T P_{\mathbf{\Psi}}^{\perp} \mathbf{r}. \tag{41}$$

Like the TCIMF, (39) can be further extended to detect multiple target signatures $\mathbf{d}_1, \mathbf{d}_2, \ldots, \mathbf{d}_{n_{\mathbf{D}}}$ in $\mathbf{D}$. In this case, (41) is generalized to

$$\delta^{\mathrm{ISP}}(\mathbf{r}) = \mathbf{1}_{n_{\mathbf{D}} \times 1}^T \left(\mathbf{D}^T P_{\mathbf{\Psi}}^{\perp} \mathbf{D}\right)^{-1} \mathbf{D}^T P_{\mathbf{\Psi}}^{\perp} \mathbf{r} \tag{42}$$

where $\mathbf{1}_{n_{\mathbf{D}} \times 1}$ is the unity vector defined in (32).

IV. Experiments

Two sets of experiments were conducted in this section, computer simulations and real hyperspectral images. The computer simulations were designed to study comparative analysis among various approaches based on SN, OSP, SBN, and SDIN models. The real hyperspectral image experiments were used to evaluate the performance of the SDIN model-based approaches in comparison with SN and SBN model-based methods.

A. Computer Simulation

The used dataset included five AVIRIS reflectance signatures, blackbrush, creosote leaves, dry grass, red soil, and sagebrush, as shown in Fig. 1. The blackbrush was considered as the desired target signature $\mathbf{d}$ with $n_D = 1$, while the creosote and sagebrush were treated as undesired target signatures $\mathbf{u}_1$ and $\mathbf{u}_2$, respectively. Furthermore, the red soil and dry grass were designated as background signatures $\mathbf{b}_1$ and $\mathbf{b}_2$, respectively. However, they could be regarded as interference signatures and denoted as $\boldsymbol{\pi}_1$ and $\boldsymbol{\pi}_2$ in SDIN model. A set of 425 mixed pixels was simulated according to Table I. Only eight pixels at pixel number 50, 100, 150, 200, 250, 300, 350, and 400 were simulated to contain abundance fractions of the desired target signature $\mathbf{d}$ (blackbrush). Another four pixels at pixel number 25, 125, 225, and 325 were simulated to contain abundance fractions of undesired target signatures, $\mathbf{u}_1$ and $\mathbf{u}_2$ (creosote and sagebrush). Except for these 12 pixels all the remaining simulated pixels contained only background signatures, $\mathbf{b}_1$ and $\mathbf{b}_2$ with 50% red soil and 50% dry grass. In addition, Gaussian noise was also added to each pixel to achieve a 30 : 1 SNR. The four detection methods, GLRT, Thai–Healey method, CEM-based method, and ISP-based approach, were evaluated for comparative analysis.

TABLE I
Abundance Fractions of 425 Simulated Pixels Used in Computer Simulations

Pixel Index	Blackbrush (desired)	Creosote (undesired)	Sagebrush (undesired)	Redsoil (background)	Drygrass (background)
50	0.2			0.4	0.4
100	0.4			0.3	0.3
150	0.6			0.2	0.2
200	0.8			0.1	0.1
250	0.2	0.35	0.35	0.05	0.05
300	0.4	0.25	0.25	0.05	0.05
350	0.6	0.15	0.15	0.05	0.05
400	0.8	0.05	0.05	0.05	0.05
25		0.2		0.4	0.4
125		0.4		0.3	0.3
225			0.2	0.4	0.4
325			0.4	0.3	0.3

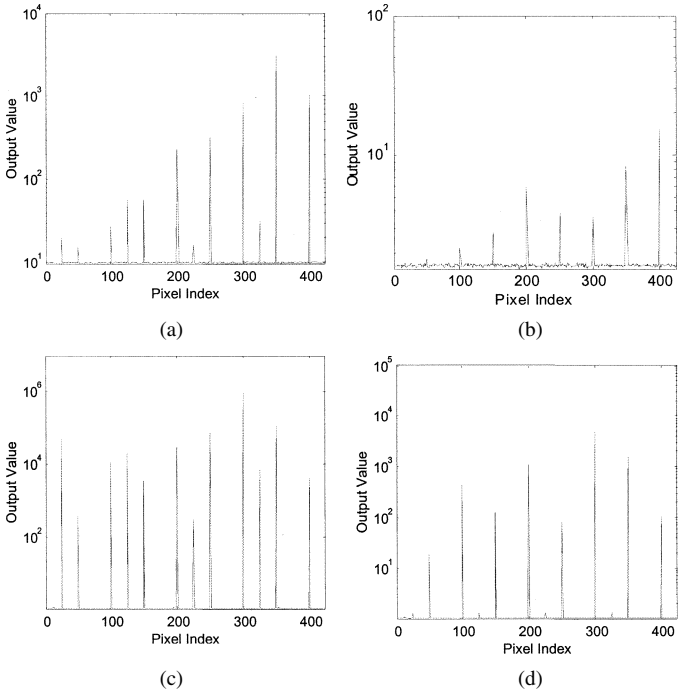

Fig. 2. GLRT detector using different models. (a) SN model. (b) OSP model. (c) SBN model. (d) SDIN model.

Example 1: Complete Target Knowledge Is Known A Priori: The computer simulations considered in this example assumed that, the knowledge of all the five signatures $\mathbf{d}$, $\mathbf{u}_1$, $\mathbf{u}_2$, $\boldsymbol{\pi}_1$, and $\boldsymbol{\pi}_2$ were known *a priori*. Fig. 2 shows the detection results using the GLRT detectors based on SN, OSP, SBN, and SDIN models. It should be noted that the output values of the

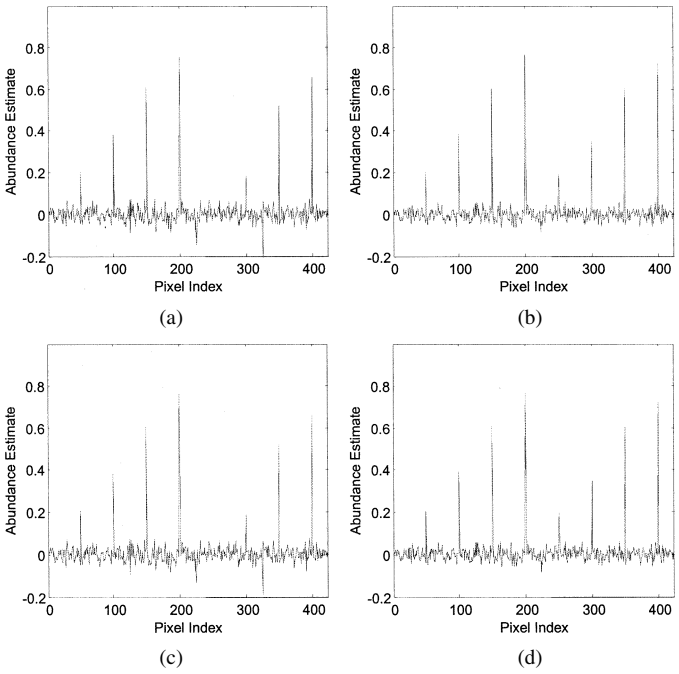

Fig. 3. CEM detector using different models. (a) SN model. (b) OSP model. (c) SBN model. (d) SDIN model.

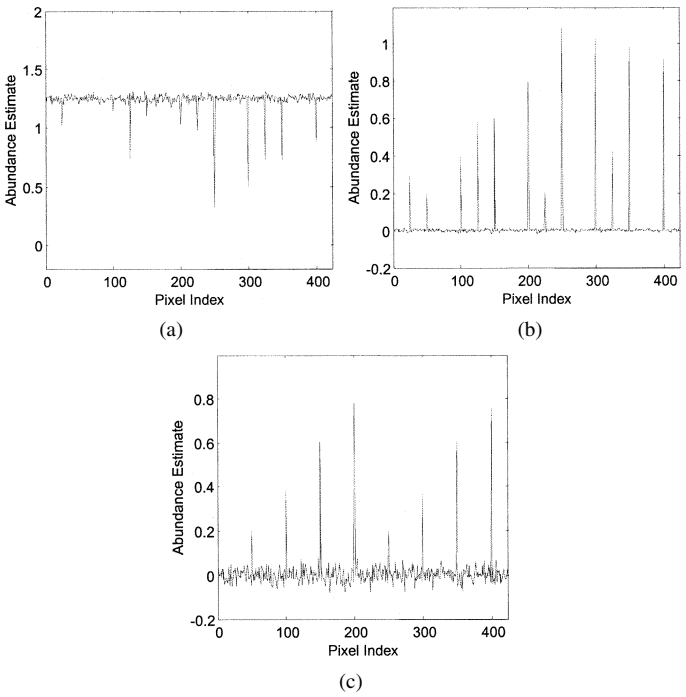

Fig. 4. ISP detector using different models. (a) OSP model. (b) SBN model. (c) SDIN model.

GLRT-based detectors are not abundance fraction estimates of blackbrush contained in simulated pixels. As shown in Figs. 2(a) and 2(c), all the four false alarms occur at pixel numbers 25, 125, 225, and 325, which contain undesired target signatures. In particular, Fig. 2(c) indicates that the SBN model did not offer any advantage over the SN model in improving detection performance. Fig. 2(b) and 2(d) shows the detection results using the OSP and SDIN model, where all the pixels that contain blackbrush were detected with no false alarm.

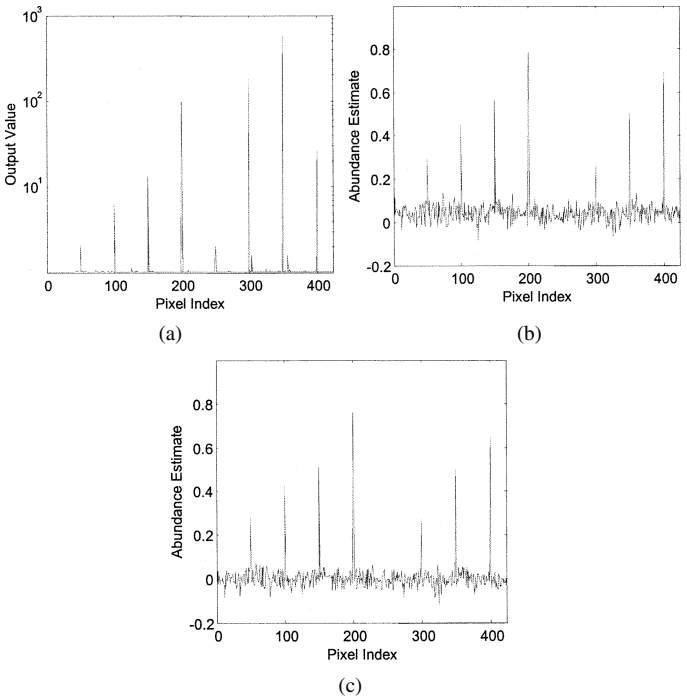

Fig. 5. Detection results using the SDIN model-based techniques when interference is unknown (SNR $= 30 : 1$). (a) GLRT. (b) TCIMF. (c) ISP.

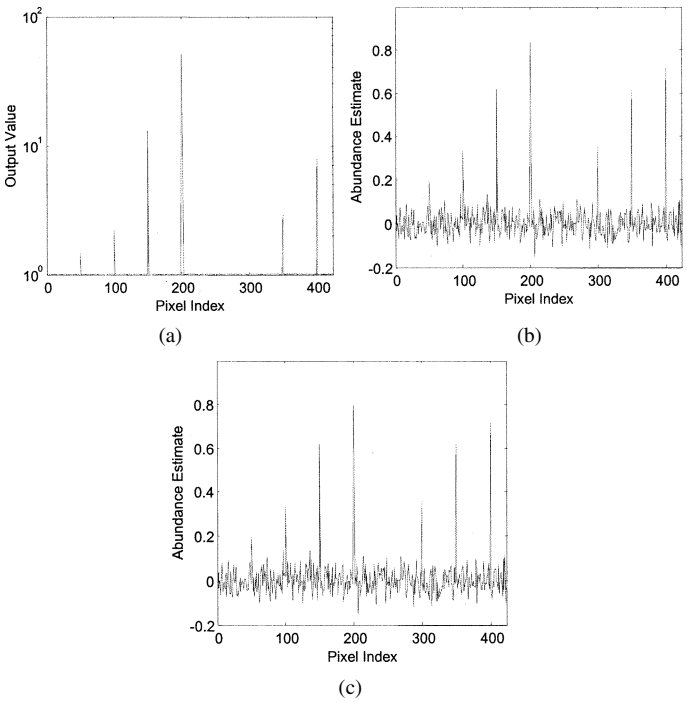

Fig. 6. Detection results using the SDIN model-based techniques when interference is unknown (SNR $= 15 : 1$). (a) GLRT. (b) TCIMF. (c) ISP.

Fig. 3(a) and (b) shows detection results using the CEM and TCIMF detector. The result in Fig. 3(a) was obtained by the CEM detector with the blackbrush as the desired target signature $\mathbf{d}$, where only the pixel at number 250 that contains blackbrush was not detected. Fig. 3(c) was obtained by the TCIMF using the SBN model, which constrained the output of the background signatures $\{\mathbf{b}_1, \mathbf{b}_2\} = \{\text{dry grass, red soil}\}$ to zero. Comparing Fig. 3(c) to (a), both results were very close and there was no

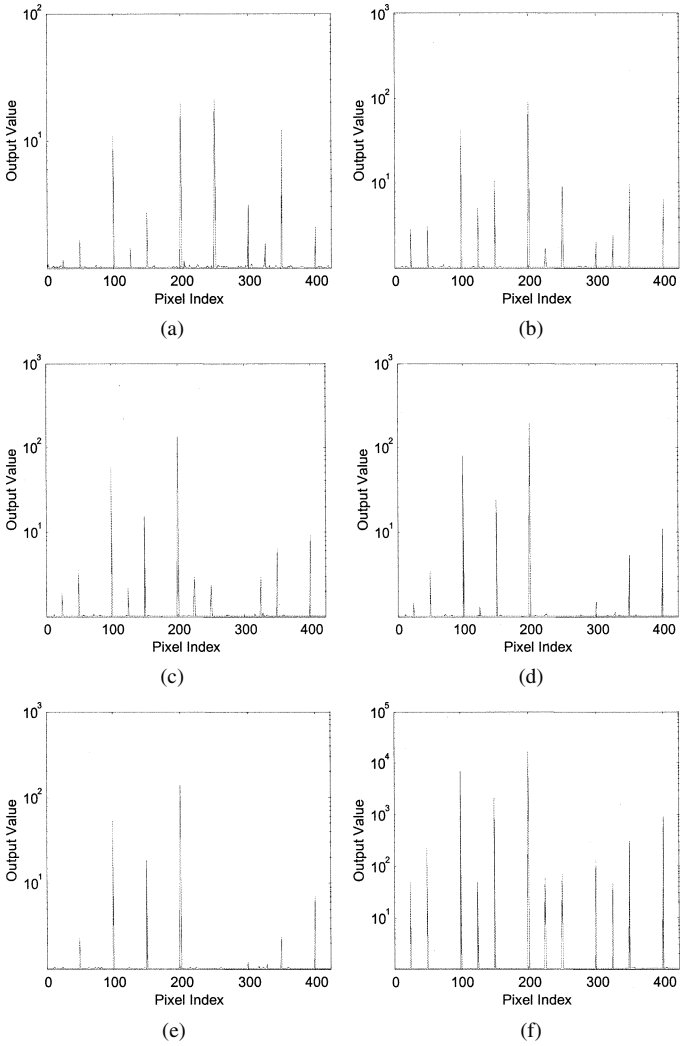

Fig. 7. Thai–Healey method using different γ_0 (SNR $= 30 : 1$). (a) $\gamma_0 = 0.999$. (b) $\gamma_0 = 0.995$. (c) $\gamma_0 = 0.99$. (d) $\gamma_0 = 0.98$. (e) $\gamma_0 = 0.97$. (f) $\gamma_0 = 0.96$.

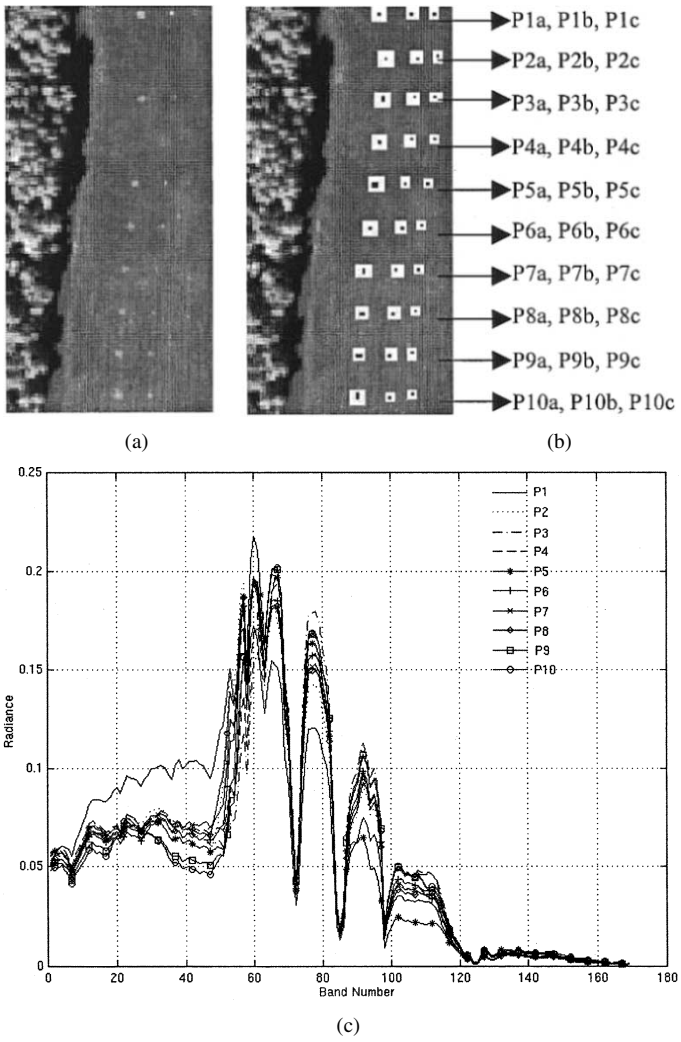

Fig. 8. (a) HYDICE image scene that contains 30 panels. (b) Spatial locations of 30 panels provided by ground truth. (c) Sectra of P1, P2, P3, P4, P5, P6, P7, P8, P9, and P10.

improvement in detection. Fig. 3(b) and (d) were obtained by the TCIMF using the OSP and SDIN model, respectively. In Fig. 3(b), the TCIMF constrained the undesired target signatures $\{\mathbf{u}_1, \mathbf{u}_2\} = \{\text{creosote, sagebrush}\}$ to zero, while minimizing the interfering effects resulting from the background signatures, $\{\mathbf{b}_1, \mathbf{b}_2\} = \{\text{dry grass, red soil}\}$ and noise. In Fig. 3(d) the TCIMF constrained all the signatures in $\mathbf{\Psi}$ that includes the undesired target signatures and background signatures, {creosote, sagebrush, red soil, dry grass}, to zero, while minimizing noise effects. As shown in Fig. 3(b) and (d), the detection results were very close and all the eight pixels that contained the blackbrush were detected.

Fig. 4(a)–(c) shows the detection results of the ISP-based detectors using the OSP model, SBN model, and SDIN model. It should be noted that the SN model is not applicable in this case. Fig. 4(a) was the OSP result. Since the background signatures were not suppressed, none of the eight pixels containing blackbrush were detected. In Fig. 4(b), the eight pixels that contained the blackbrush as well as the four pixels that contained undesired target signatures $\{\mathbf{u}_1, \mathbf{u}_2\} = \{\text{creosote, sagebrush}\}$ were all detected. This was due to the fact that only the background signatures {red soil, dry grass} were rejected by the SBN model. Fig. 4(c) shows the detection result by implementing the ISP approach with the SDIN model, where all the undesired signatures and background signatures {creosote, sagebrush, red soil, dry grass} were effectively annihilated, while the eight pixels containing blackbrush were detected. This example demonstrates an advantage of using the SDIN model over the OSP and SBN models.

Example 2: Only the Knowledge of Blackbrush Is Known A priori: The same set of 425 simulated pixels used in Example 1 was also used for Example 2. However, unlike Example 1, Example 2 assumed that only the knowledge of the blackbrush was provided *a priori* and designated as the desired signature $\mathbf{d}$. No other prior knowledge is available. So in this case we need to estimate interference signatures. It should be noted that since there is no prior knowledge other than blackbrush, all the unknown signatures (i.e., creosote leaves, sagebrush) would be treated as interferers regardless of whether they were background sources or undesired signatures.

First, the number of spectrally distinct target signatures was estimated as $n_{\mathbf{D}} + n_{\mathbf{U}} + n_{\Pi} = 4$. Since the blackbrush was known, $n_{\mathbf{D}} = 1$ and $n_{\mathbf{U}} + n_{\Pi} = 3$. The algorithm presented

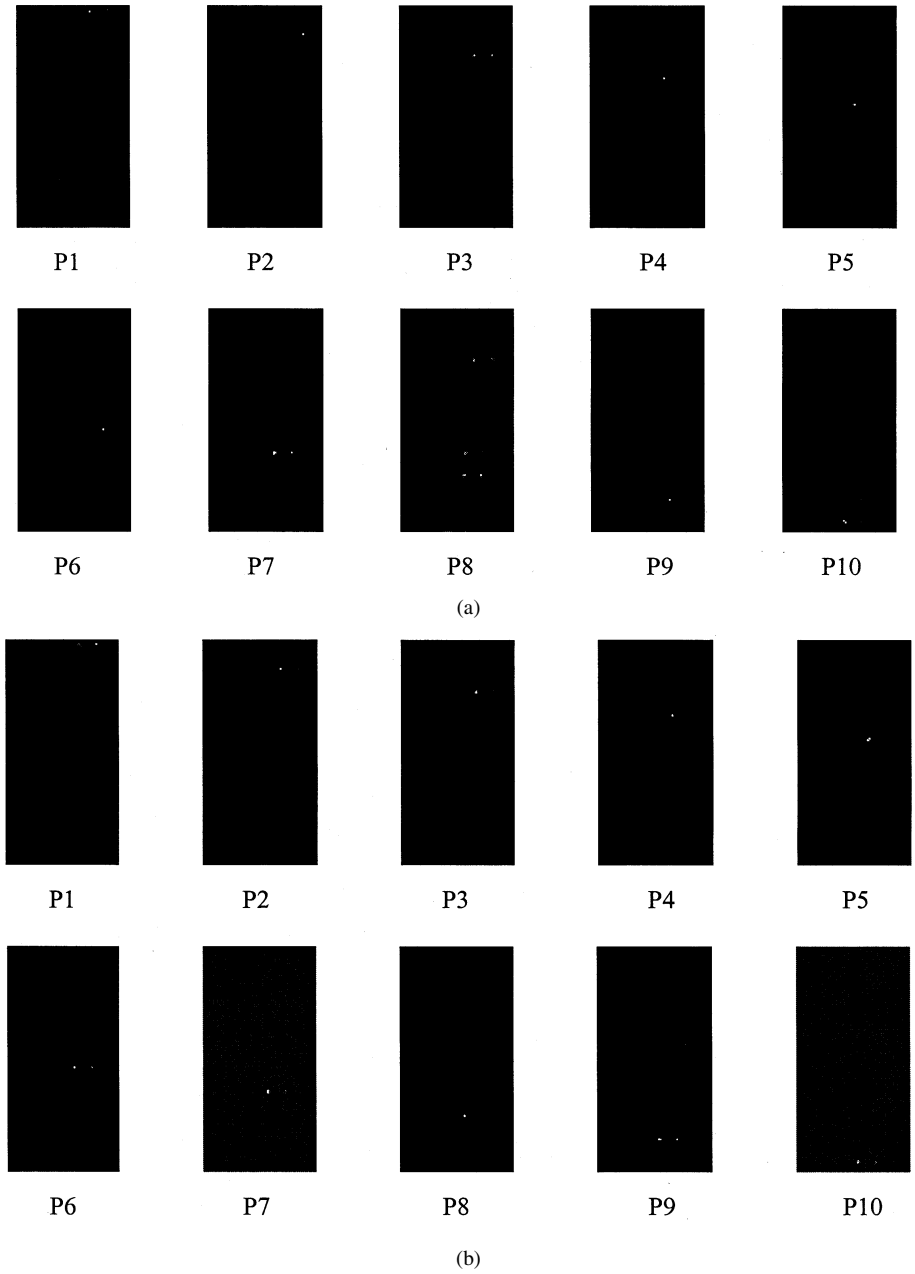

Fig. 9. Detection results with GLRT method for HYDICE experiment. (a) OSP model. (b) SDIN model.

in Section II-B was applied to find 3 signatures other than the blackbrush. These three found signatures were pixels at 214, 250, and 34, which were considered as interference signatures and would be annihilated in detection. Fig. 5(a) shows the GLRT detection result, where all the eight pixels containing blackbrush were detected correctly, while the four interference pixels were also successfully rejected. However, there were also two false alarms at pixels 304 and 357. Fig. 5(b) and (c) was obtained by the TCIMF and the ISP approach with the SDIN model, respectively. Both of figures detected seven of these eight pixels, but missed the pixel at 250. This is due to the fact that the pixel at 250 contained only 20% blackbrush, but 35% of each of undesired target signatures, creosote leaves and sagebrush which were considered as interferers. As a result of interference annihilation, this pixel was nulled out effectively. However, the detection results were not as good as their counterparts in Example 1, because the knowledge of interference signatures that was provided in Example 1 was not given in this example. For the case when the SNR was reduced to $15:1$, Fig. 6(a)–(c) shows the results of the GLRT and ISP with the SDIN model and TCIMF, respectively. The performance of the TCIMF and the ISP in Fig. 6(b) and (c) was slightly degraded but nearly remained the same as that when SNR $= 30:1$. The GLRT did not perform as well as it did for SNR $= 30:1$ in Fig. 5(a) and missed the detection of the pixels at 250 and 300 as shown in Fig. 6(a). The above experiments showed that the GLRT could be very effective detector if the SDIN model is used instead of the SN model. A major disadvantage of the GLRT is that its output values do not represent the abundance estimates of target signatures. Compared to the ISP and the TCIMF which are essentially abundance estimators, the GLRT can be used for detection only. That is why the GLRT outperformed the ISP and TCIMF in Figs. 5 and 6 in

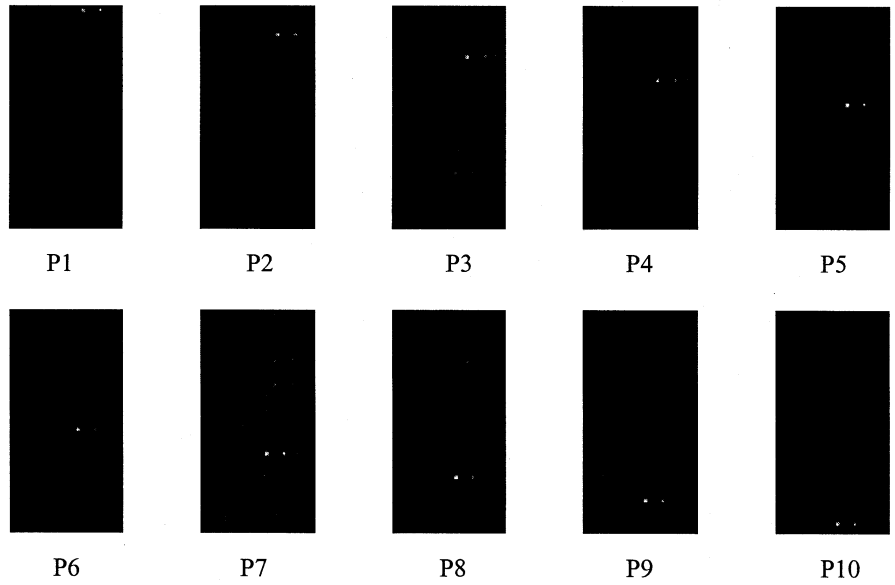

(a)

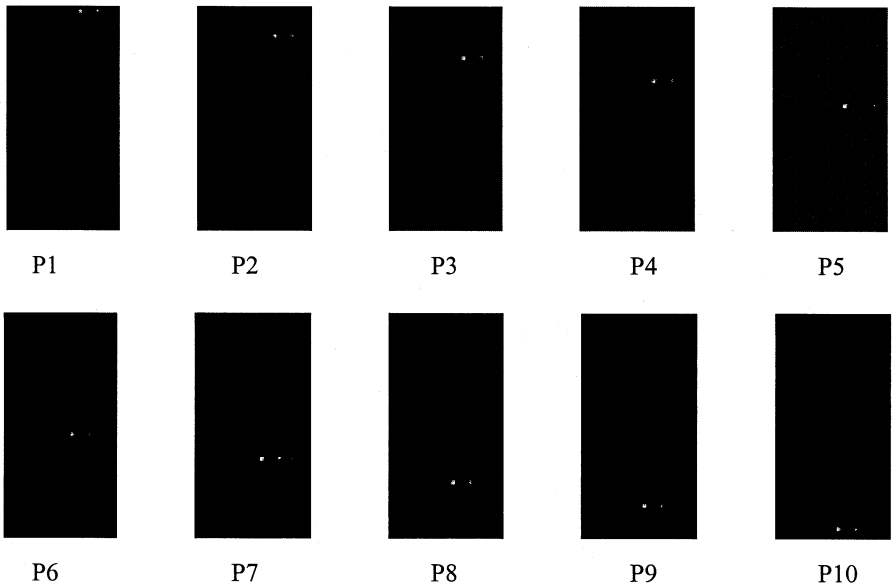

(b)

Fig. 10. Detection results with TCIMF method for HYDICE experiment. (a) OSP model. (b) SDIN model.

terms of target detection where both the ISP and TCIMF tried to estimate the abundance fractions of the blackbrush contained in the pixels.

In order to apply the Thai–Healey method, we need to construct the background data matrix $\mathbf{Y}$. In this case, we first must find all target candidate pixels whose signatures were similar and close to the desired signature $\mathbf{d}$, blackbrush, where the criterion defined by (22) was used for similarity measure. Then, the matrix $\mathbf{Y}$ was formed by all the image pixels except the found target pixels. The first $n_{\langle \mathbf{B} \rangle}$ eigenvectors of the matrix $\mathbf{Y}$ were then used to construct the background subspace $\langle \mathbf{B} \rangle$. $n_{\langle \mathbf{B} \rangle} = 10$ was found to be appropriate in our simulations. Fig. 7(a)–(f) shows the detection results with six different thresholds set by $\gamma_0 = 0.999, 0.995, 0.99, 0.98, 0.97$, and 0.96. Fig. 7(a) is the result obtained when $\gamma_0 = 0.999$, where three pixels at 300, 350, and 400 were removed from being considered in $\mathbf{Y}$. When $\gamma_0 = 0.995$ was used, two more pixels at 200 and 250 were removed and the result is shown in Fig. 7(b). Similarly, with $\gamma_0 = 0.99$ the pixels at 125 and 150 were further removed; then the two more pixels at 100 and 325 were removed after γ_0 was reduced to 0.98. This is followed by an additional pixel at 25 to be removed with $\gamma_0 = 0.97$. Finally, when γ_0 reached 0.96, the pixels at 50 and 225 were further removed, in which case all the eight desired target pixels at 50, 100, 150, 200, 250, 300, 350, and 400 and interferer pixels at 25, 125, 225, and 325 were removed. When γ_0 was in the range of 0.9496 and 0.96, no other pixels were picked up. According to our experiments, when γ_0 was between 0.9473 and 0.9496, different background pixels were removed. As long as γ_0 is below 0.9473, all the 425 pixels were removed. As shown in these figures, none of

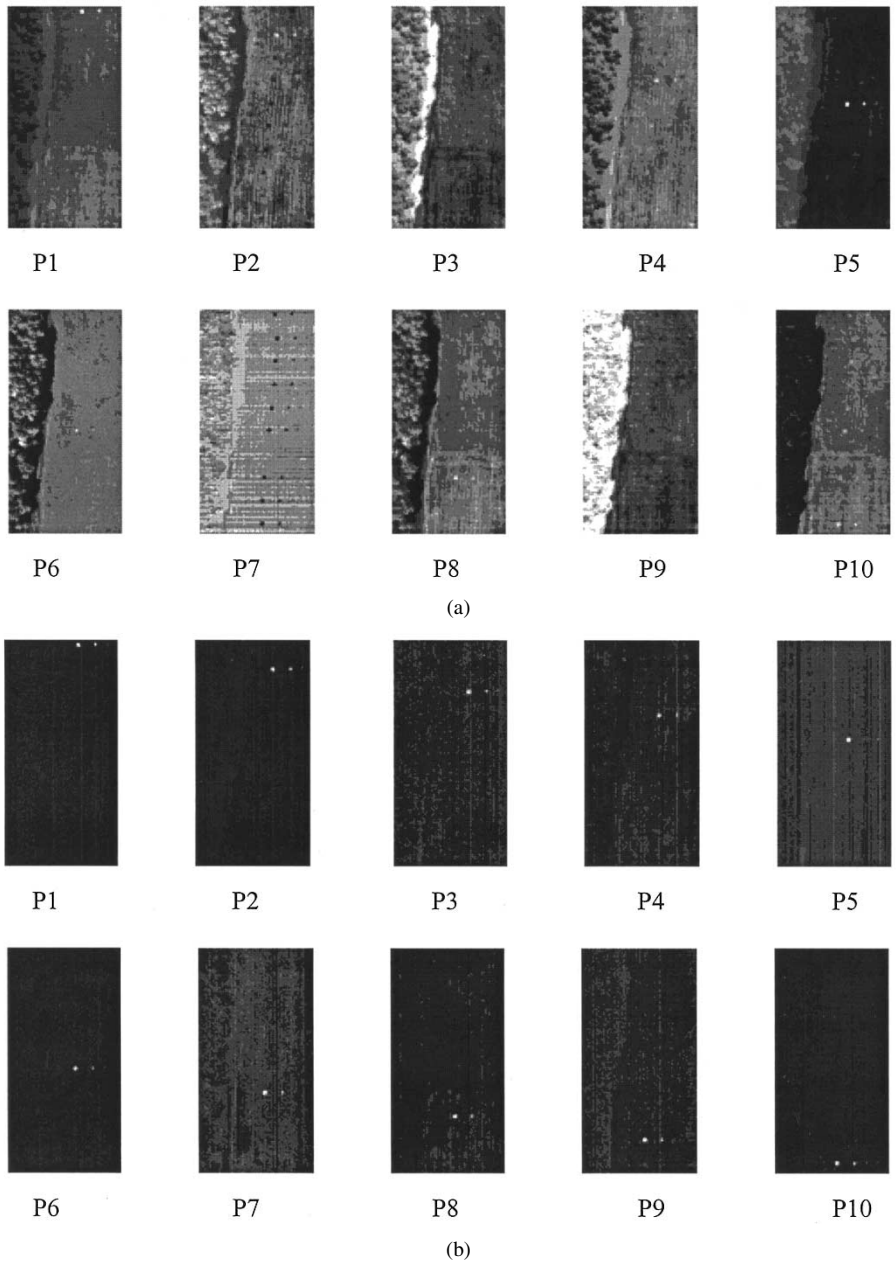

Fig. 11. Detection results with ISP method for HYDICE experiments. (a) OSP model. (b) SDIN model.

them provided good detection results. Nevertheless, Fig. 7(a) and (e) seemed among the best, because Fig. 7(a) detected the eight blackbrush pixels but also extracted two interferers at 125 and 325, while Fig. 7(e) detected six out of the eight pixels containing blackbrush as well as rejected the four interferer pixels. A comparison among Figs. 5–7 demonstrates that the SDIN model-based approaches performed better than the SBN model-based Thai–Healey method in all the cases. Similar experiments were also conducted for the case of SNR $= 15 : 1$. The detection results were not as good as that presented here. This was due to the fact that all the pixels were mixed, and it was difficult to remove the desired blackbrush $\mathbf{d}$ from the background data matrix $\mathbf{Y}$ to effectively construct the background subspace. On the other hand, the SDIN model-based GLRT, ISP, and TCIMF approaches performed better because of two reasons: 1) The unsupervised target generation process, i.e., ATDCA algorithm [4], [5], was used to find and locate spectrally distinct signatures, which was effective; and 2) the SDIN model allows us to eliminate the *a posteriori* signals sources to improve target detection.

B. Hyperspectral Image Experiments

The data used in the experiments is the Hyperspectral Digital Imagery Collection Experiment (HYDICE) data. The image scene of size 128×64 shown in Fig. 8(a) was collected in Maryland in 1995 from the flight altitude of 10 000 ft with approximately 1.5 m GSD. Removing bands with low SNR ratio results in 169 dimensions. There are 30 panels present in the image scene which are arranged in a 10×3 matrix. Each element in this matrix is denoted by p_{ij} with row indexed by i and column indexed by j. The three panels in the same row were made from the same material and are of size 3 m $\times$ 3 m, 2 m $\times$ 2 m, and

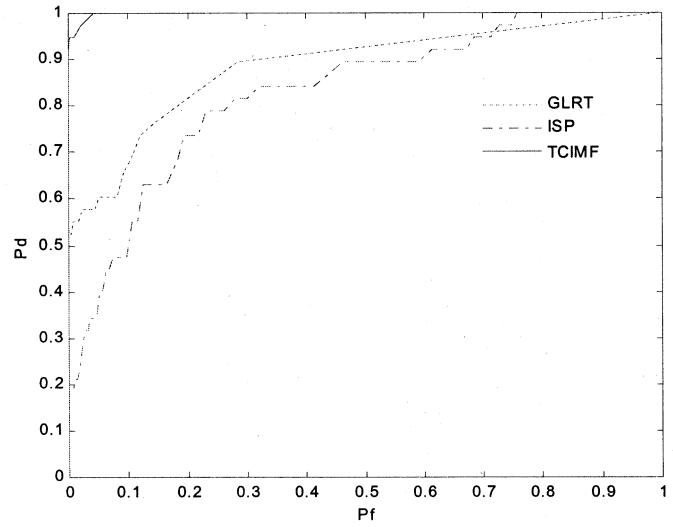

(a)

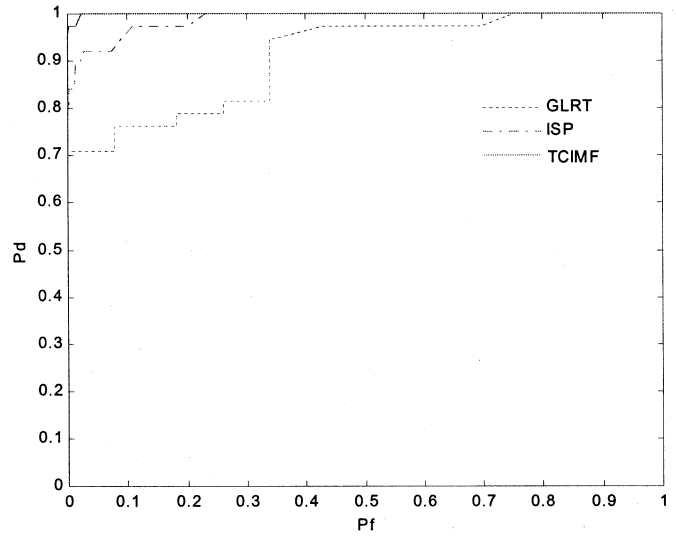

(b)

Fig. 12. ROC curves. (a) OSP model. (b) SDIN model.

1 m × 1 m, respectively. The ground truth map is provided in Fig. 8(b) and shows the precise spatial locations of panel pixels. Here, the black pixels are referred to as panel center pixels, and white pixels are considered as panel pixels mixed with background pixels. Fig. 8(c) plots the spectra of these ten panel signatures, $\{P_i\}_{i=1}^{10}$, generated by averaging black pixels in each row. We can see that the panel signatures are very similar. In addition to panel signatures, two background signatures were also generated from the grass field and tree line to the left of the panels. Using this 30-panel HYDICE scene we can compare the performance among the four methods implemented with the OSP model and the SDIN model, since the undesired panel signatures are known *a priori*.

First of all, the number of interferers was estimated by the eigenthresholding method in Section II-A, which was $n_{\mathbf{D}} + n_{\mathbf{U}} + n_{\Pi} = 27$. The interference finding algorithm in Section II-B was then used to generate the interference signatures. Figs. 9–11 show the detection results using the GLRT, the TCIMF, and the ISP with the OSP model and SDIN model, respectively. As we can see from these figures, using the OSP model in Figs. 9(a), 10(a), and 11(a) produced more false alarms than using the SDIN model in Figs. 9(b), 10(b), and 11(b). For instance, Fig. 9(a) shows the results of the GLRT with the OSP model where P3 and P7 were also detected when detecting P8; the CEM in Fig. 10(a) picked up some abundance fraction of P4 when detecting P2; and Fig. 11(a) is for the ISP with the OSP model where the background signatures could not be well suppressed. In general, the TCIMF with the SDIN model seemed to provide the best results.

TABLE II
DETECTION RATES RESULTING FROM THE OSP MODEL

# of interfering signatures	GLRT	ISP	TCIMF
0	0.8807	0.8246	0.9930

TABLE III
DETECTION RATES RESULTING FROM THE SDIN MODEL

# of interfering signatures	GLRT	ISP	TCIMF
10	0.9183	0.9620	0.9941
15	0.9348	0.9696	0.9942
20	0.9047	0.9827	0.9942
25	0.9080	0.9856	0.9946
30	0.9394	0.9849	0.9946

In order to calculate detection ability of each method, the receiver operating characteristic (ROC) curves were plotted in Fig. 12 for the three methods using the OSP model and SDIN model. It was created based on plots of detection probability versus false-alarm probability. Since the images resulting from the ISP and TCIMF are estimated abundance fractional images which are gray scale, it requires a threshold value to segment targets from the images. The plotted ROC curves were produced by using abundance percentage $a\%$ as a threshold value from 100% down to 0%. In other words, the abundance fractions of target signatures detected in the ISP-generated and TCIMF-generated images were normalized to the interval [0, 1]. Then, these normalized abundance fractions were thresholded by $a\%$ with a running through from 100 down to 0. Once ROC curves were generated, the area under each ROC curve, referred to as detection rate (DR) in this paper (A_z in [25]), was calculated and tabulated in Tables II and III. The DR can be used to evaluate the effectiveness of each detector. The higher the DR, the better the detector. So when the DR is 1, the detector is an ideal detector. Conversely, when DR $= 0.5$, the detector performs the worst. The ROC curves in Fig. 12 demonstrate that the SDIN model-based detection methods outperformed their OSP model-based counterparts, because the SDIN model took care of the interference, while the SN model does not. Additionally, it also showed that the TCIMF was the best among the

four detection methods and GLRT was the worst according to DR in Tables II and III. The detection results using the ISP and TCIMF largely remained unchanged with various $n_{\mathbf{U}} + n_{\Pi}$. As for GLRT, it was sensitive to the number of interference signatures, and a large $n_{\mathbf{U}} + n_{\Pi}$ does not guarantee better detection.

Since the ROC results generated by the SBN model-based and SDIN model-based Thai–Healey methods are very close, they are nearly the same by visual inspection. In this case, we calculated their detection rates instead. Tables IV–VI tabulate the DR for different number of eigenvectors $n_{\langle \mathbf{B} \rangle}$ and various similarity thresholds, where the values of $n_{\langle \mathbf{B} \rangle}$ labeled by "*" were obtained by Thai–Healey method in [15] with two thresholds set to $t_1 = 4.8 \times 10^{-5}$ and $t_2 = 3.9 \times 10^{-5}$. We can see that the detection results were sensitive to t_1 and t_2, and the SDIN model-based Thai–Healey method performed slightly better than its SBN-based counterpart. This experiment demonstrated that Thai–Healey method can be improved using the SDIN model. Compared to the SDIN-based GLRT, ISP, and TCIMF methods, Thai–Healey method produced better results than did GLRT and ISP, and slightly worse than did TCIMF. This is because the panel pixels studied in this experiment are pure pixels, where $n_{\langle \mathbf{B} \rangle}$ and γ_0 can be appropriately determined for an effective background subspace $\langle \mathbf{B} \rangle$.

TABLE IV
DETECTION RATES RESULTING FROM THAI-HEALEY'S METHOD WITH $\gamma = 0.990$

# of eigenvectors $n_{\mathbf{B}}$	SBN	SDIN
5	0.9812	0.9874
10	0.9943	0.9943
15	0.9941	0.9945
20*	0.9943	0.9944

TABLE V
DETECTION RATES RESULTING FROM THAI-HEALEY'S METHOD WITH $\gamma = 0.995$

# of eigenvectors $n_{\mathbf{B}}$	SBN	SDIN
5	0.9935	0.9939
10	0.9812	0.9941
15	0.9942	0.9944
20*	0.9943	0.9943

TABLE VI
DETECTION RATES RESULTING FROM THAI-HEALEY'S METHOD WITH $\gamma = 0.998$

# of eigenvectors $n_{\mathbf{B}}$	SBN	SDIN
5	0.9940	0.9941
10	0.9813	0.9942
15*	0.9943	0.9944

V. CONCLUSION

In this paper, we presented a signal-decomposed and interference-annihilated approach to enhance hyperspectral target detection. Several main contributions are summarized as follows.

1) In order to implement the SDIA approach, a new sensor signal model, called a signal-decomposed/interference/noise model, was introduced, which categorized signals into *a priori* and *a posteriori* signal sources, and considered interference and noise as separate information sources. This model allows us to deal with the interference separately such that their interfering effects can be effectively eliminated in target detection.
2) In order to determine *a posteriori* signal sources, a two-step technique was proposed, i.e., an eigenthresholding-technique-based Neyman–Pearson detection theory followed by an unsupervised target generation algorithm to find potential *a posteriori* signal sources.
3) Three SDIN model-based SDIA approaches were investigated. In particular, the original SN model-based generalized-likelihood ratio test approach was extended to an SDIN model-based approach. The other two approaches are SDIN model-based interference subspace projection and SDIN model-based CEM. All these three SDIN model-based SDIA methods along with Thai–Healey method were analyzed and evaluated through a comprehensive study of computer simulations and real HYDICE data. As demonstrated by experiments, SDIN model-based methods generally outperform their counterparts using the SN, OSP, and SBN models.
4) The signal/background/noise model-based Thai–Healey method was extended using the SDIN model. It is found that that the SDIN model-based detectors generally provide better results than those based on the SBN model.

As a concluding remark, although the ATDCA is proposed in our SDIA approach to find and locate *a posteriori* signal sources, it does not imply that it is the only algorithm that can be used for this purpose. As a matter of fact, any unsupervised algorithms can be implemented in conjunction with the SDIA approach as long as they can effectively find *a posteriori* signal sources, such as a least squares error-based algorithm in [5, ch. 5].

REFERENCES

[1] C.-I Chang, E. Sun, and M. L. G. Althouse, "An unsupervised interference rejection approach to target detection and classification for hyperspectral imagery," *Opt. Eng.*, vol. 37, no. 3, pp. 735–743, 1998.
[2] C.-I Chang and Q. Du, "Interference and noise adjusted principal components analysis," *IEEE Trans. Geosci. Remote Sensing*, vol. 37, pp. 2387–2396, Sept. 1999.
[3] C. Brumbley and C.-I Chang, "An unsupervised vector quantization-based target signature subspace projection approach to classification and detection in unknown background," *Pattern Recognit.*, vol. 32, no. 7, pp. 1161–1174, July 1999.
[4] H. Ren and C.-I Chang, "Automatic spectral target recognition in hyperspectral imagery," *IEEE Trans. Aerosp. Electron. Syst.*, vol. 39, pp. 1232–1249, Oct. 2003.
[5] C.-I Chang, *Hyperspectral Imaging: Techniques for Spectral Detection and Classification*. Amsterdam, The Netherlands: Kluwer, 2003, ch. 13.
[6] J. C. Harsanyi and C.-I Chang, "Hyperspectral image classification and dimensionality reduction: an orthogonal subspace projection," *IEEE Trans. Geosci. Remote Sensing*, vol. 32, pp. 779–785, July 1994.

[7] J. B. Adams, M. O. Smith, and P. Johnson, "Spectral mixture modeling: A new analysis of rock and soil types at the Viking Lander 1 suite," *J. Geophys. Res.*, vol. 91, no. B8, pp. 8098–8112, July 10, 1986.
[8] A. R. Gillespie, M. O. Smith, J. B. Adams, S. C. Willis, A. F. Fischer, III, and D. E. Sabol, "Interpretation of residual images: spectral mixture analysis of AVIRIS images Owens valley, California," in *Proc. 2nd AVIRIS Workshop*, 1990, pp. 243–270.
[9] A. F. H. Goetz and J. W. Boardman, "Quantitative determination of imaging spectrometer specifications based on spectral mixing models," in *Proc. IGARSS*, 1989, pp. 1036–1039.
[10] D. E. Sabol, J. B. Adams, and M. O. Smith, "Quantitative sub-pixel spectral detection of targets in multispectral images," *J. Geophys. Res.*, vol. 97, pp. 2659–2672, 1992.
[11] J. B. Adams, M. O. Smith, and A. R. Gillespie, "Image spectroscopy: interpretation based on spectral mixture analysis," in *Remote Geochemical Analysis: Elemental and Mineralogical Composition*, C. M. Pieters and P. A. Englert, Eds. Cambridge, U.K.: Cambridge Univ. Press, 1993, pp. 145–166.
[12] L. Scharf and B. Friedlander, "Matched subspace detector," *IEEE Trans. Signal Processing*, vol. 42, pp. 2146–2157, Aug. 1994.
[13] S. Kraut, L. Scharf, and L. T. McWhorter, "Adaptive subspace detector," *IEEE Trans. Signal Processing*, vol. 49, no. 12, pp. 3005–3014, 2001.
[14] Y. Zhang and M. C. Amin, "Array processing for nonstationary interference suppression in DS/SS communications using subspace projection techniques," *IEEE Trans. Signal Processing*, vol. 49, pp. 3005–3014, Dec. 2001.
[15] B. Thai and G. Healey, "Invariant subpixel material detection in hyperpsectral imagery," *IEEE Trans. Geosci. Remote Sensing*, vol. 40, pp. 599–608, Mar. 2002.
[16] C.-I Chang, X. Zhao, M. L. G. Althouse, and J.-J. Pan, "Least squares subspace projection approach to mixed pixel classification in hyperspectral images," *IEEE Trans. Geosci. Remote Sensing*, vol. 36, pp. 898–912, May 1998.
[17] H. Ren and C.-I Chang, "Target-constrained interference-minimized approach to subpixel target detection for hyperspectral imagery," *Opt. Eng.*, vol. 39, no. 12, pp. 3138–3145, Dec. 2000.
[18] J. C. Harsanyi, "Detection and Classification of Subpixel Spectral Signatures in Hyperspectral Image Sequences," Ph.D. dissertation, Dept. Elect. Eng., Univ. Maryland Baltimore County, Baltimore, MD, 1993.
[19] W. H. Farrand and J. C. Harsanyi, "Mapping the distribution of mine tailing in the coeur d'Alene river valley, Idaho, through the use of constrained energy minimization technique," *Remote Sens. Environ.*, vol. 59, pp. 64–76, 1997.
[20] C.-I Chang and Q. Du, "Estimation of number of spectrally distinct signal sources in hyperspectral imagery," *IEEE Trans. Geosci. Remote Sensing*, vol. 42, pp. 608–619, Mar. 2004.
[21] R. E. Roger and J. F. Arnold, "Reliability estimating the noise in AVIRIS hyperspectral images," *Int. J. Remote Sens.*, vol. 17, no. 10, pp. 1951–1962, 1996.
[22] T. W. Anderson, *An Introduction to Multivariate Statistical Analysis*, 2nd ed. New York: Wiley, 1984.
[23] H. V. Poor, *An Introduction to Signal Detection and Estimation*, 2nd ed. Berlin, Germany: Springer-Verlag, 1994.
[24] C.-I Chang, Q. Du, T. S. Sun, and M. L. G. Althouse, "A joint band prioritization and band decorrelation approach to band selection for hyperspectral image classification," *IEEE Trans. Geosci. Remote Sensing*, vol. 37, pp. 2631–2641, Nov. 1999.
[25] C. E. Metz, "ROC methodology in radiological imaging," *Invest. Radiol.*, vol. 21, pp. 720–723, 1986.

Qian Du (S'98–M'00) received the Ph.D. degree in electrical engineering from the University of Maryland Baltimore County, Baltimore, in 2000.

She is currently an Assistant Professor in the Department of Electrical Engineering and Computer Science, Texas A&M University, Kingsville. Her research includes image processing, pattern classification, remote sensing, and neural networks.

Dr. Du is a member of SPIE and Phi Kappa Phi.

Chein-I Chang (S'81–M'87–SM'92) received the B.S. degree from Soochow University, Taipei, Taiwan, R.O.C., in 1973, the M.S. degree from the Institute of Mathematics, National Tsing Hua University, Hsinchu, Taiwan, in 1975, and the M.A. degree from the State University of New York, Stony Brook, in 1977, all in mathematics. He received the M.S and M.S.E.E. degrees from the University of Illinois at Urbana-Champaign in 1982 and the Ph.D. degree in electrical engineering from the University of Maryland, College Park, in 1987.

He has been with the University of Maryland Baltimore County (UMBC), Baltimore, since 1987, as a Visiting Assistant Professor from January 1987 to August 1987, Assistant Professor from 1987 to 1993, Associate Professor from 1993 to 2001, and Professor in the Department of Computer Science and Electrical Engineering since 2001. He was a Visiting Research Specialist in the Institute of Information Engineering at the National Cheng Kung University, Tainan, Taiwan, from 1994 to 1995. He has a patent on automatic pattern recognition and several pending patents on image processing techniques for hyperspectral imaging and detection of microcalcifications. His research interests include automatic target recognition, multispectral/hyperspectral image processing, medical imaging, information theory and coding, signal detection and estimation, and neural networks. He is the author of a book *Hyperspectral Imaging: Techniques for Spectral Detection and Classification* (Norwell, MA: Kluwer). He is on the editorial board and was the Guest Editor of a special issue on telemedicine and applications of the *Journal of High Speed Networks*.

Dr. Chang received a National Research Council Senior Research Associateship Award from 2002–2003 at the U.S. Army Soldier and Biological Chemical Command, Edgewood Chemical and Biological Center, Aberdeen Proving Ground, MD. He is an Associate Editor in the area of hyperspectral signal processing for the IEEE TRANSACTION ON GEOSCIENCE AND REMOTE SENSING. He is a Fellow of SPIE and a member of Phi Kappa Phi and Eta Kappa Nu.